This is a “preproof” accepted article for *Mineralogical Magazine*.
This version may be subject to change during the production process.
10.1180/mgm.2025.10

Nancyrossite, $FeGeO_6H_5$, a new hydroxyperovskite

M.D. Welch[1]*, J. Najorka[1], A.K. Kleppe[2], A.R. Kampf[3], J. Spratt[1]

[1]Natural History Museum, London, SW7 5BD, UK.

[2]Diamond Light Source UK, Harwell Science and Innovation Campus, Didcot, UK.

[3]Mineral Sciences Department, Natural History Museum of Los Angeles County, 900 Exposition Boulevard, Los Angeles, CA90007, USA.

*Corresponding author: m.welch@nhm.ac.uk

Abstract

Nancyrossite, ideally $FeGeO_6H_5$, is a new hydroxyperovskite from Tsumeb. It likely formed by the oxidation and partial dehydrogenation of stottite, $FeGe(OH)_6$, with which it is intimately associated. The structure of nancyrossite has been determined in tetragonal space group $P4_2/n$: a = 7.37382(12) Å, c = 7.29704(19) Å, V = 396.764(16) Å^3, Z = 4, R_1(all) = 0.034, wR_2(all) = 0.051, GoF = 1.057. Empirical formulae of two crystals have almost end-member compositions, $Fe^{3+}_{1.01}Zn_{0.03}Ge_{0.98}O_6H_5$ and $Fe^{3+}_{1.01}Zn_{0.04}Ge_{0.98}O_6H_5$. Structure determination indicates that 88% Fe is ferric. The chemical formula proposed here for nancyrossite recognizes that although H atoms form OH groups, writing the formula as $FeGeO(OH)_5$ implies that one of the six oxygen atoms is very underbonded, with a bond-valence sum of only ~1.2 v.u. As such, H in nancyrossite may have novel crystal chemistry. For example, the five H atoms may be distributed dynamically over the six O atoms, a phenomenon that would be averaged by X-ray diffraction, and so go undetected. Nancyrossite is the Ge-analogue of jeanbandyite. By analogy with nancyrossite, we propose

revision of the ideal formula of jeanbandyite from $FeSnO(OH)_5$ (Welch and Kampf, 2017) to $FeSnO_6H_5$.

Introduction

The crystal chemistry of hydroxyperovskites has been reviewed by Mitchell et al. (2017). The key structural features are (i) the absence of a cavity *A* cation, (ii) all oxygens form hydroxyl groups and (iii) each oxygen is an H donor and acceptor. The absence of a cavity cation and the moderately strong hydrogen bonding leads to highly rotated octahedra.

There are two distinct groups: (a) single hydroxyperovskites with trivalent cations only and stoichiometry $B(OH)$; (b) double hydroxyperovskites with stoichiometry $BB'(OH)_6$, where *B* is a monovalent or divalent cation and *B′* is a tetravalent or pentavalent cation. Polymorphism involving cubic and tetragonal structures has been observed in $Ga(OH)_3$ and $MnSn(OH)_6$. In double hydroxyperovskites *B* and *B′* octahedra alternate.

Different hydrogen bonding configurations occur in hydroxyperovskites depending upon space group and octahedra tilt system. For example, cubic structures with space groups $Pn\bar{3}$ and $Im\bar{3}$ have three equal in-phase tilts $a^+ a^+ a^+$ that lead to isolated 4-membered rings of ···O-H···O-H··· linkages. Crankshafts composed of hydrogen-bonded bridges occur in tetragonal, orthorhombic and monoclinic hydroxyperovskites in combination with isolated 4-membered O-H···O-H rings or zig-zag chains.

There are fifteen known natural hydroxyperovskites: eight stannates, one antimonate, $Fe(OH)_3$ (bernalite), $In(OH)_3$ (dzahlindite), $Ga(OH)_3$ (söhngeite), and three germanates (stottite, zincostottite and nancyrossite), all of which are exceptionally rare minerals. Only one hydroxyperovskite with $B^+B'^{5+}(OH)_6$ stoichiometry is known: mopungite $NaSb(OH)_6$.

Here, we report the discovery of a new double hydroxyperovskite and member of the stottite subgroup that is unusual in having five rather than the usual six H per formula: nancyrossite $FeGeO_6H_5$. The mineral honours Prof. Nancy L. Ross, mineral physicist and mineralogist at Virginia Polytechnic Institute, Blacksburg, Virginia, USA. Nancy Ross has made major contributions to our knowledge of the crystal chemistry, thermochemistry and crystallography of perovskites and related phases, including stottite. The mineral and name have been approved by the International Mineralogical Association (2024-033; Welch *et al*. 2024).

Experimental methods

Sample

The sample containing stottite and nancyrossite was donated to MDW by the mineral collector and mineralogist William Pinch of Rochester, New York, U.S.A. This sample, which comprises only loose crystals, also contains grains of sphalerite and galena and is from the germanium horizon at Level 30 of the Tsumeb mine, Namibia (19°15'S, 17°42'E), the type locality of stottite. In addition to broken crystals, stottite occurs in the sample as large cuboidal crystals up to 1 mm in diameter. Occasionally, larger crystals sometimes display stepped surfaces that are likely due to etching or growth phenomena. The new mineral described herein, nancyrossite, occurs as subhedral grains or fragments up to 0.3 mm maximum dimension, that do not display stepped surfaces.

While selecting stottite crystals for a high-pressure study, numerous honey-coloured crystals were found that differed from the usual greenish yellow of stottite. These were screened by SCXRD and found to have a much smaller unit cell than stottite, e.g. 396.76(2) $Å^3$, 396.66(2) $Å^3$ *versus* 425.22(2) $Å^3$. Structure determination by single-crystal X-ray

diffraction (SCXRD) indicated that the FeO_6 octahedron of the honey-coloured phase was much smaller than that of stottite and was consistent with a dominantly ferric state for Fe. As such, this phase was recognized as a new mineral, and its formal description is given here.

Three separate crystals were used in the characterisation of nancyrossite (crystals #7, #8 and #9). Crystals #7 and #8, for which crystal structures were determined, were used for analysis by electron microprobe and are mounted together on a glass slide. The full structure of crystal #9 is reported here. All three crystals are very similar and have almost identical structural and chemical data; they are deposited in the mineral collection of the Natural History Museum, London, UK, catalogue numbers BM2024,1, BM2024,2 and BM2024,3 for crystals #9 (holotype), #7 and #8, respectively.

Electron microprobe analysis

Two co-type crystals (#7 and #8) were mounted in epoxy and polished for electron microprobe analysis. Wavelength-dispersive analysis was done using a Cameca SX100 electron microprobe with an accelerating potential of 20 kV, a current of 20 nA and a 5 μm beam. Standards used are given in Table 1. A preliminary survey using energy-dispersive analysis indicated that the only metals present are Zn, Fe, Ge. Notably, Mn and Sn were below detection limits. The H content of nancyrossite could not be determined using chemical methods, because not enough material is available (5 small crystals). Consequently, the H content is deduced from the crystal structure reported here. No suitable material was available for Mössbauer spectroscopy. Divalent and trivalent iron contents were deduced from the crystal structure, as described below.

Optical properties

The holotype crystal (#9) was used for determination of optical properties. The determination of RI values using a spindle stage was problematic because the refractive indices were above 1.8, the limit for accurate measurement in the stage's optical cell due to the opacity (darkness) of the high-RI liquids needed. Optic axial angle (2V) was measured and determined using extinction data analysed with EXCALIBURW (Gunter *et al*. 2004). Conoscopic figures were consistent with the measured high 2V.

As is also the case with stottite (tetragonal, $P4_2/n$), nancyrossite displays anomalous biaxial optics. Jeanbandyite, cubic $Pn\bar{3}$, has anomalous uniaxial optics (Kampf, 1982). Birefringence values for $\beta - \alpha$ and $\gamma - \beta$ were obtained using a Berek compensator. These values taken with those estimated using the Gladstone-Dale equation based upon the crystal structure determination of crystal #9 allows a meaningful description of the optical characteristics of nancyrossite.

Raman spectroscopy

Unpolarized Raman spectra were collected for crystals #8 (before mounting for electron microprobe) and #9. These crystals were placed on the culet of an ultra-low fluorescence diamond and spectra recorded over the range 100–3900 cm^{-1}. The instrument used was the LabRAM HR800 (Horiba Jobin Yvon) at beamline I15, Diamond Light Source, UK. It was equipped with 1200g grating, a 20x objective, and an electrically cooled CCD detector. Excitation of each crystal used the 532-nm line of a 300 mW Torus laser focused down to a 10 μm spot on the sample and collected through a 75 μm confocal aperture using a 180° back-scattering geometry. Laser power at the sample position varied between 3-4 mW; exposure times were 2x 120 sec. The intrinsic resolution of the spectrometer is <1.0 cm^{-1} and

calibrations are accurate to ±1 cm^{-1}. The frequency of each Raman band was obtained by fitting Voigtian line profiles using a least-squares algorithm.

X-ray diffraction

Quasi-powder X-ray diffraction data were collected for crystal #9 using a Gandolfi-type movement (ϕ and ω circles) on a Rapid II diffractometer (Rigaku Oxford Diffraction) operated at 45 kV and 36 mA, equipped with a curved image plate and graphite monochromatized Cu*K*α radiation. Diffraction patterns were processed using the 2DP program (Rigaku-Oxford Diffraction) and the HighScore Plus program (Malvern Panalytical, Degen *et al*., 2014).

Single-crystal XRD was carried out using an *Xcalibur* four-circle single-crystal diffractometer (Rigaku-Oxford Diffraction) equipped with a 1K *Eos* area detector and graphite-monochromated Mo*K*α radiation. Data collection and data reduction used the *Crysalis* program (©Rigaku Oxford Diffraction). Raw intensities were corrected for Lorentz, polarization and absorption effects, and converted to structure factors. A multi-scan absorption correction was applied. Crystal structure determination used SHELX (Sheldrick, 2015), as detailed in the Results section.

Results

Chemical formula

Empirical formulae of nancyrossite crystals #7 and #8, calculated on the basis of six O^{2-} + five H^{+}, are: $Fe^{3+}_{1.01}Zn_{0.03}Ge_{0.98}O_6H_5$ (#7) and $Fe^{3+}_{1.01}Zn_{0.04}Ge_{0.98}O_6H_5$ (#8). The % H_2O values shown in Table 1 were calculated for both average formulae for 2.5 H_2O (5 H *apfu*). The simplified formula is $(Fe^{3+},Zn)GeO_6H_5$. The ideal chemical formula is $FeGeO_6H_5$ which requires Fe_2O_3 34.80, GeO_2 45.59, H_2O 17.48, total 100 wt.%. The values for stottite,

$FeGe(OH)_6$, are (%): FeO 31.18, GeO_2 45.39, H_2O 23.42, total 100 wt.%. The empirical values are clearly closer to those of nancyrossite than stottite. The ferric state of Fe in nancyrossite is demonstrated by crystal structure determination and bond-valence calculations, as described below. The rationale for writing the ideal chemical formula as $FeGeO_6H_5$ is given in the Discussion section ("chemical formula") with particular reference to jeanbandyite.

Optical properties

As noted above, the refractive indices of nancyrossite are very high and precluded direct determination using heavy liquids. The alternative approach outlined above gave the following properties: $\beta - \alpha = 0.005$ (meas.), $\gamma - \beta = 0.003$ (meas); bi.axial (–): $\alpha = 1.966$ (calc.), $\beta = 1.971$ (calc.), $\gamma = 1.974$ (calc.); Gladstone-Dale $n_{av} = 1.97$; $2V_{meas} = 73.5(4)°$, $2V_{calc} = 75.4°$; dispersion r < v slight; orientation X = **c**; non-pleochroic.

Raman spectroscopy

Raman spectra of nancyrossite crystal #8 and jeanbandyite (Hingston Quarry, Cornwall) are shown in Figure 3(a). These spectra in the (OH)-stretching region are very similar, comprising two broad bands at approximately 2850 and 3150 cm^{-1}. The Raman spectrum of stottite from Tsumeb studied by Kleppe *et al*. (2012) is shown in Figure 3(b) and comprises five resolved bands that lie within the envelope defined by the nancyrossite and jeanbandyite spectra. High FWHM values for Raman and infrared bands spectra in the (OH)-stretching region is characteristic of hydroxyperovskites, e.g. 60-110 cm^{-1}. Typical oxygen-oxygen donor-acceptor distances of hydroxyperovskites are 2.7-2.8 Å (Table 7), implying

weak hydrogen bonding. Hence, it is unlikely that the high FWHM values are due to significant anharmonicity of the O-H bond in these structures. The origin of the high FWHMs remains to be determined.

Powder X-ray diffraction

Calculated and measured d_{hkl} values and their intensities are shown in Table 2. Refined unit cell parameters (tetragonal, space group $P4_2/n$) are a = 7.3770(1) Å, c = 7.2977(1) Å, V = 397.149(9) Å^3; R(profile) = 0.019, wR(profile) = 0.030, GoF =1.221.

Crystal structure: SCXRD

The structures of three nancyrossite crystals (#7, #8, #9) were determined in space group $P4_2/n$ using SHELX (Sheldrick, 2015). The refined structures of all crystals are very similar. The structure of the holotype (#9) is reported here and is representative of the structures of all nancyrossite crystals studied. Only eight very weak violators of the *n*-glide and screw tetrad were present, all having $I/\sigma(I) < 0.6$. Consequently, $P4_2/n$ is considered the correct choice of space group. An attempt to refine in non-centrosymmetric space group $P4_2$, described below, clearly indicated that a centrosymmetric structure is the correct choice, i.e. space group $P4_2/n$.

Neutral scattering factors for Fe, Ge, O and H were used (Wilson, 1992). Refinement of site scattering at the Fe site confirmed that it is fully occupied by Fe and so the occupancy was not refined thereafter (occ. = 100% Fe). Minor merohedral twinning (minor twin = 8%) was detected during the early stages of refinement and this was incorporated into the refined structure model. A soft restraint of 0.85 ±0.05 Å for the O-H bond was used for the

refinement of H atom positions; the isotropic displacement parameters U_{iso} , of all H atoms were linked and refined as a single variable.

Results are summarized in Tables 3–8. A CIF for the holotype crystal (#9), including structure factors, is deposited with the journal. A summary comparing unit cell parameters, refinement indices and geometric parameters for crystals #7, #8 and #9 is shown in Table 6.

It is important to realise that it is now possible to recognise partially occupied H sites using SCXRD when crystals of high quality are available, e.g. fully occupied *versus* half-occupied H sites (e.g. Lafuente *et al*. 2015; Welch and Kleppe, 2016; Welch *et al*. 2024). For example, in the early stages of refinement of the stottite ($P4_2/n$), the unmodelled residual electron-density in the difference-Fourier map given in the Q-list output by SHELX for a H-free model contains five maxima that correspond to one full and four partially occupied H sites that can be identified based upon O-H distance (0.8–0.9 Å for XRD) and O-H···O configuration (oxygen donor-acceptor distance and approximate O-H···O angle). Taken together with O-H distances, the highly directional O-H (non-bifurcated) hydrogen bonds of hydroxyperovskites allow plausible H positions to be checked and refined. This approach successfully located the five non-equivalent half-occupied sites of nancyrossite.

Iron, Ge and all five non-equivalent O atoms were found by Direct Methods and then refined by full-matrix least-squares. Plausible sites for all five H atoms were found (Table 4, Fig. 2). These sites are analogous to those of stottite except for the occupancy of the four-membered ring site H1, which appears to be half-occupied in nancyrossite (fully occupied in stottite). Hence, the five non-equivalent H sites in nancyrossite, all on general positions of multiplicity 8, are half occupied in the $P4_2/n$ model. This result is consistent with 5 H atoms per formula unit ($Z = 4$): ¼ × (5 × ½ × 8) = 5 H apfu.

One of the two non-equivalent octahedra of nancyrossite has a volume of 9.05 Å^3 and a geometry almost identical to that of the GeO_6 octahedron of stottite (9.07 Å^3). It is much smaller than the SnO_6 octahedra of stannate hydroxyperovskites such as wickmanite $MnSn(OH)_6$ (11.57Å^3) and burtite $CaSn(OH)_6$ (11.48 Å^3). The other octahedron of nancyrossite is much smaller (11.08 Å^3) than the Fe^{2+}, Mn^{2+} and Mg octahedra of related hydroxyperovskites (Table 9); it is much closer to the value of the $Fe^{3+}O_6$ octahedron of bernalite $Fe(OH)_3$ (10.8 Å^3). Electron microprobe analysis (Table 1) confirms that the two octahedra are occupied by Fe and Ge. The small size of the Fe octahedron is consistent with occupancy by Fe^{3+} not Fe^{2+} (Table 7). Assuming a linear variation of the volume of the FeO_6 octahedron with Fe^{2+}/Fe^{3+} between stottite and bernalite, a value of 11.08 Å^3 implies that the Fe site is 88% Fe^{3+}. A calculation using *OccQP* (Wright et al. 2000), which uses site scattering values and bond valences, gives $0.897Fe^{3+}$:$0.103Fe^{2+}$, in almost exact agreement with the result obtained using the bernalite/stottite V_{oct} correlation.

Structure refinement of crystal #9 in non-centrosymmetric space group $P4_2$ (#77) was also attempted to test the robustness of the centrosymmetric ($P4_2/n$) model. Iron, Ge and all six non-equivalent oxygen positions appeared at the structure solution stage and stable refinement of these atoms was achieved. However, a Flack parameter of 0.46(12) and very high correlations between atoms related by a missing centre of symmetry clearly indicated that a centrosymmetric structure (i.e. $P4_2/n$) is the correct choice. Six plausible H sites were also apparent in the difference-Fourier maps at later stages of the refinement of the $P4_2$ structure. However, the refined overall U_{iso} of these six sites was non-positive definite and it was not possible to refine the structure further.

A data collection at 100 K for a cotype crystal (MDW1) was made to see if any further information on H locations could be found. An excellent refinement in space group $P4_2/n$ was obtained: R_1(all) = 0.026, wR_2(all) = 0.054, *GoF* = 1.130. However, only three of

the five H sites were located with certainty, all with half occupancy, i.e. the ring H site and two of the half-occupied crankshaft sites. It is, nonetheless, significant that the ring site refines more satisfactorily as half occupied in nancyrossite, unlike stottite for which full occupancy of this site is found consistently for different crystals (MDW, unpublished data).

Details of the hydrogen bonding in nancyrossite and stottite are shown in Table 7. In nancyrossite, the shortest O_D–O_A distances, 2.697 Å and 2.700 Å, are associated with the O(3)H(1)···O(3) of the ring and the O(2)H(5)···O(2) of the crankshaft, respectively. The longest O_D–O_A distance (2.968 Å) is O(1)H(3)···O(1) of the crankshaft. In stottite, the shortest O_D–O_A distances are for the O(3)H(1)···O(3) of the ring (2.734 Å) and O(2)H(5)···O(2) of the crankshaft (2.716 Å); the longest O_D–O_A distance is for O(1)H(3)···O(1) of the crankshaft (2.953 Å) as in nancyrossite distance (2.968 Å). Overall, there is close correspondence between O_D–O_A distances in nancyrossite and stottite.

Bond valence calculations

Bond valence sums, BVS, for Fe, Ge and O atoms of nancyrossite were calculated using the parameters of Brese and O'Keeffe (1991) and are shown in Table 8(a). These calculations confirm that Fe occurs as Fe^{3+} (BVS 2.91 v.u.) rather than Fe^{2+} (2.72 v.u.). Oxygen bond valence sums range from 1.13 to 1.18 v.u. and indicate bonding to H. The same calculation for stottite is shown in Table 8(b) and it is clear that Fe is divalent (BVS 1.99 v.u.).

Discussion

Chemical formula

Crystal structure determination indicates that H atoms occur at positions that can be assigned to OH groups. However, writing the formula so as to include formal hydroxyl groups gives $FeGeO(OH)_5$, as was done by Welch and Kampf (2017) for jeanbandyite

$FeSnO(OH)_5$, and implies that one oxygen per formula is not bonded to H, which is not what is found by SCXRD, nor is it crystal-chemically reasonable as this oxygen will be very under-bonded (e.g. with a BVS of ~ 1.2 vu). In the next section we apply the same reasoning to jeanbandyite. Given the association of H with oxygen as OH groups in nancyrossite as seen by XRD, we refer to this mineral as a hydroxyperovskite.

Relations to other minerals

Table 9 summarises crystallographic data for hydroxyperovskites related to nancyrossite. Two minerals and one synthetic are particularly noteworthy with regard to nancyrossite: natanite, jeanbandyite and the synthetic analogue of the latter, reported by Nakayama *et al*. (1977) as $FeSnO(OH)_5$. The reduction in unit cell volume for natanite → $FeSnO(OH)_5$ is 33.64 Å^3 (7%). The corresponding reduction for stottite → nancyrossite is 6.5% (27.60 Å^3).

Using crystallographic and crystal-chemical arguments, Welch and Kampf (2017) revised the formula of jeanbandyite from $(Fe^{3+}_{1-x}, \square_x)(Sn_{1-y}, \square_y)(OH)_6$ (□ = vacancy) reported by Kampf (1982) to $Fe^{3+}_x M^{2+}_{1-x} Sn(OH)_{6-x}$ ($1 \geq x \geq 0.5$) with an ideal end-member formula (x = 1) of $Fe^{3+}SnO(OH)_5$. However, this formula implies that one of the six oxygen atoms of the formula is not associated with H. The behaviour of H in nancyrossite has yet to be clarified. What is clear, however, is that the crystallographic data imply five H atoms per formula in the ideal structure. Until a model for H behaviour and distribution is available, we consider it to be more appropriate to write the chemical formula of jeanbandyite as $FeSnO_6H_5$ by analogy with what we propose here for nancyrossite, $FeGeO_6H_5$.

The $Pn\bar{3}$ structure of hydroxyperovskites differs from that of tetragonal varieties by having different Glazer octahedral-tilt systems ($Pn\bar{3}$ = $a^+a^+a^+$, $P4_2/n$ = $a^+a^+c^-$) that lead to

very different hydrogen-bonding topologies (Mitchell et al. 2017). The H-bonding arrangement of the cubic structure consists only of isolated four-membered rings, whereas the tetragonal structure has alternating (002) layers of four-membered rings and crankshafts, as shown in Figure 2. Hence, the cubic topology ($a^+a^+a^+$) of jeanbandyite reported by Kampf (1982) and confirmed by Welch and Kampf (2017) is correct as it cannot be confused with a tetragonal topology that has a reversed tilt ($a^+a^+c^-$). Welch and Kampf (2017) demonstrated that refinement of the crystal structure of jeanbandyite in space group $P4_2/n$ fails to produce a satisfactory structure.

Zincostottite, ideally $ZnGe(OH)_6$, presumed to be from the same Ge-rich horizon at Tsumeb as nancyrossite, was recently approved as a new mineral (Kampf *et al*. 2024). The empirical formula reported is $Zn_{0.77}Fe^{3+}_{0.23}Ge_{1.00}O_6H_{5.77}$, with all iron in the ferric state and a corresponding H deficiency of 0.23 H *apfu* relative to the ideal formula. As such, this empirical formula can be considered a solid solution between zincostottite and nancyrossite.

The likely deprotonated site in nancyrossite is suggested by a comparison with jeanbandyite. The latter has the $Pn\bar{3}$ topology with only isolated rings, each having two non-equivalent H sites that, in the average structure found by diffraction methods, are both half occupied. The H sites of neighbouring rings are separated by a minimum distance of ~2.7 Å. Whether or not this distance is too far for H interactions between adjacent rings (hopping?) is unknown. The significance of partial occupancy of H sites in hydroxyperovskites remains to be determined.

Single crystal neutron diffraction (SCND) allows the accurate determination of occupancies of H sites. It is now possible to carry out SCND experiments on crystals with a minimum dimension of 0.1 mm. High quality crystals of nancyrossite larger than this

dimension are available, and we intend to do SCND in the near future in order to locate the partially occupied H sites more accurately than is possible using SCXRD.

Implications

Synthetic hydrogen-doped perovskites are important materials for use as protonic conductors and electrolytic catalysts. Various protonation mechanisms have been used, such as the preparation of oxygen-deficient compositions followed by hydrolysis at oxygen vacancies, e.g. $BaSc_{0.667}W_{0.333}O_3 \rightarrow BaSc_{0.8}W_{0.2}O_{2.8} \rightarrow [BaSc_{0.8}W_{0.2}O_{2.8}(OH)_{0.2} + 0.2\ H^+]$. In contrast to such "hydrogen-doped" structures which generate mobile protons, nancyrossite and jeanbandyite are already highly protonated and have vacant H sites that may facilitate proton migration or localised site hopping. Hydroxyperovskites are considered to be potentially significant electrolytic catalysts and photocatalysts (Evans et al., 2023), with possible applications in fuel cells.

Stannate hydroxyperovskites present an opportunity to prepare synthetic samples of these materials as analogues of jeanbandyite $FeSnO_6H_5$, e.g. $MnSnO_6H_5$, $CoSnO_6H_5$, $NiSnO_6H_5$. The solid solution behaviour of these materials which, in principle, could be used to tailor properties, is unexplored.

Recent studies of hydroxyperovskites have revealed interesting structural behaviour. For example, Welch and Kleppe (2016) found that natural $Ga(OH)_3$ (söhngeite) transforms on heating from a $P4_2/n$ structure to cubic $Im\bar{3}$ at ~ 380 K. This transformation involves a major reconfiguration of the hydrogen bonding topology and may be driven by proton behaviour.

Compared with perovskites *sensu stricto*, hydroxyperovskites are relatively unexplored. For example, their solid solution behaviour is largely unknown. Stannate double hydroxyperovskites can be synthesized easily, e.g. $CaCl_2 + K_2Sn(OH)_6.3H_2O \rightarrow CaSn(OH)_6$

+ 2KCl (removed by washing). Hence, there is scope for using synthetics to study solid solution behaviour.

With specific regard to hydroxyperovskites having partial H deficiencies, such as nancyrossite and jeanbandyite, the discovery of zincostottite with substantial (23 mol%) nancyrossite component (Kampf *et al*. 2024) indicates that solid solutions between $BB'(OH)_6$ and $BB'O_6H_5$ double hydroxides could be synthesized to investigate the systematics of H behaviour in these materials.

Proton conduction has been reported for synthetic $MgSn(OH)_6$ and $CoSn(OH)_6$ powders at 298-500 K (Jena *et al*. 2004). Above 523 K these compounds decompose to oxides. No attempts to measure proton conduction in natural hydroxyperovskites have been reported. Obtaining large crystals (> 100 μm minimum dimension) of high quality, such as occur for nancyrossite and stottite, will allow the study of H conduction directly. Thus, there is considerable opportunity and motivation for exploring the crystal chemistry and properties of hydroxyperovskites.

Acknowledgements

MDW acknowledges the generosity of the late Bill Pinch of Rochester, New York State, in donating the superb sample from Tsumeb containing stottite and nancyrossite for research. We thank Callum Hatch at NHM, London for preparing the polished section of the single crystals for EMPA.

REFERENCES

Brese, N.E. and O'Keeffe, M. (1991) Bond-valence parameters for solids. *Acta Crystallographica* **B47**, 192-197.

Degen, T., Sadki, M., Bron, E., König, U. and Néner, G. (2014) The *HighScore* suite. *Powder Diffraction*, **29** (Supplement 2), S13-S18.

Evans, H.A. Wu, Y. Seshadri, R. and Cheetham, A.K. (2020) Perovskite-related ReO3 materials. *Nature Reviews Materials*, **5**, 196-213.

Gunter, M.E., Bandli, B.R., Bloss, F.D., Evans, S.H., Su, S.C. and Weaver, R. (2004) Results from a McCrone spindle stage short course, a new version of EXCALIBR, and how to build a spindle stage. *The Microscope* **52**, 23–39.

Jena, H., Kutty, K.V.G. and Kutty T.R.N. (2004) Ionic transport and structural investigations of $MSn(OH)_6$ (M = Ba, Ca, Mg, Co, Zn, Fe, Mn). *Materials Chemistry and Physics*, **88**, 167–179.

Kampf, A.R. (1982) Jeanbandyite, a new member of the stottite group from Llallagua, Bolivia. *Mineralogical Record* **13**, 235–239.

Kampf, A.R., Désor, J., Welch, M.D., Ma, C. and Möhn G. (2025) Zincostottite, the zinc analogue of stottite from Tsumeb, Namibia. *Mineralogical Magazine* (in press).

Kleppe, A.K., Welch. M.D., Crichton, W.A. and Jephcoat, A.P. (2012) Phase transitions in hydroxyperovskites: a Raman spectroscopic study of stottite, $FeGe(OH)_6$ to 21 GPa. *Mineralogical Magazine* **76**, 949-962.

Lafuente, B., Yang, H. and Downs, R.T. (2015) Crystal structure of tetrawickmanite $Mn^{2+}Sn(OH)_6$. *Acta Crystallographica* **E71**, 234-237.

Mitchell, R.H., Welch, M.D. and Chakmouradian. A.R. (2017) Nomenclature of the perovskite supergroup: A hierarchical system of classification based on crystal structure and composition. *Mineralogical Magazine* **81**, 411-461.

Nakayama, N., Kosuge, K. and Kach, S. (1977) Magnetic properties of $FeSn(OH)_6$ and its oxidation product $FeSnO(OH)_5$. *Materials Research Bulletin* **13**, 17-22.

Robinson, K., Gibbs, G.V. and Ribbe, P.H. (1971) Quadratic elongation: a quantitative measure of distortion in coordination polyhedra. *Science* **172**, 567-570.

Sheldrick, G.M. (2015) Crystal structure refinement with SHELXL. *Acta Crystallographica* **C71**, 3-8.

Welch, M.D. and Kampf, A.R. (2017) Stoichiometric partially-protonated states in hydroxyperovskites: the jeanbandyite enigma revisited. *Mineralogical Magazine* **81**, 297–303.

Welch, M.D. and Kleppe, A.K. (2016) Polymorphism of the hydroxyperovskite $Ga(OH)_3$ and possible proton-driven transformational behaviour. *Physics and Chemistry of Minerals* **43**, 515-526.

Welch, M.D., Crichton, W.A. and Ross, N.L. (2005) Compression of the perovskite-related mineral bernalite $Fe(OH)_3$ to 9 GPa and a reappraisal of its structure. *Mineralogical Magazine* **69**, 309–315.

Welch, M.D., Najorka, J. and Wunder, B. (2024) Crystal structure, hydrogen bonding, and high-pressure behaviour of the hydroxyperovskite $MgSi(OH)_6$: A phase relevant to the deep subduction of hydrated oceanic crust. *American Mineralogist* **109**, 255–264.

Welch, M.D., Najorka, J., Kleppe, A.K., Kampf, A.R. and Spratt. J. (2024) Nancyrossite, IMA 2024-033. CNMNC Newsletter 81, Eur. J. Mineral., 36 (in press).

Wilson, A.J.C. (editor) (1992) Mathematical, Physical and Chemical Tables. *International Tables for Crystallography, Volume C.* Kluwer Academic Publishers, Dordrecht, The Netherlands.

Wright, S.E., Foley, J.A., and Hughes, J.M. (2000) Optimization of site occupancies in minerals

using quadratic programming. *American Mineralogist*, **85**, 524–531.

FIGURE CAPTIONS

Figure 1. Photomicrograph of a composite grain (left) comprising distinct nancyrossite (Ncy) and stottite (Sto) components; to the right of this composite grain is a larger single stottite crystal. SCXRD shows that the two crystals of the composite grain have structural continuity of their lattices whereby *a* and *c* axes are coincident. The outer surface of the composite grain shows growth steps also commonly seen in stottite and jeanbandyite, likely due to etching. The different colours of the two minerals are evident.

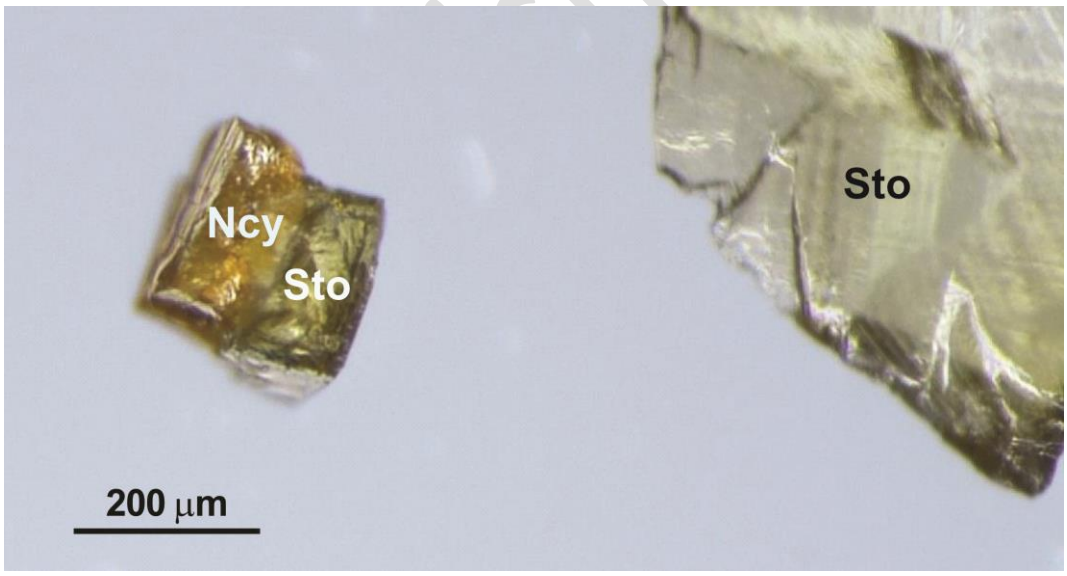

Figure 2. Structures of nancyrossite and wickmannite. Tetragonal structures such as nancyrossite and stottite have two in-phase and one out-of-phase (reverse) tilts of octahedra; cubic structures such as wickmanite and natanite have three equal in-phase tilts. These different tilt systems lead to different hydrogen bonding connectivities. Cubic structures have only isolated 4-membered rings of O-H…O bridges whereas tetragonal structures have O-H…O crankshafts and isolated O-H…O rings. **(a)** the ring of stottite with a fully occupied H1 site; **(b)** the ring of nancyrossite with a half-occupied H1 site; **(c)** the crankshaft shared by stottite and nancyrossite structures with four half-occupied non-equivalent H sites**; (d)** the nancyrossite structure projected onto (001) showing the reverse tilt parallel to [001]; **(e)** the nancyrossite structure projected onto (010) showing the in-phase tilts, and a single in-plane crankshaft shown as a red line; **(f)** the wickmanite structure ($Pn\bar{3}$) showing the in-phase tilts along all three axes. Examples of the orientations of rings (blue) and crankshafts (brown) are shown. An example of in-plane ring is shown for nancyrossite as a blue square in Fig. (d); an example of an in-plane ring in wickmanite is shown as an outlined red square in Fig. (f). Crankshafts extend parallel to the *x* and *y* axes of nancyrossite and stottite.

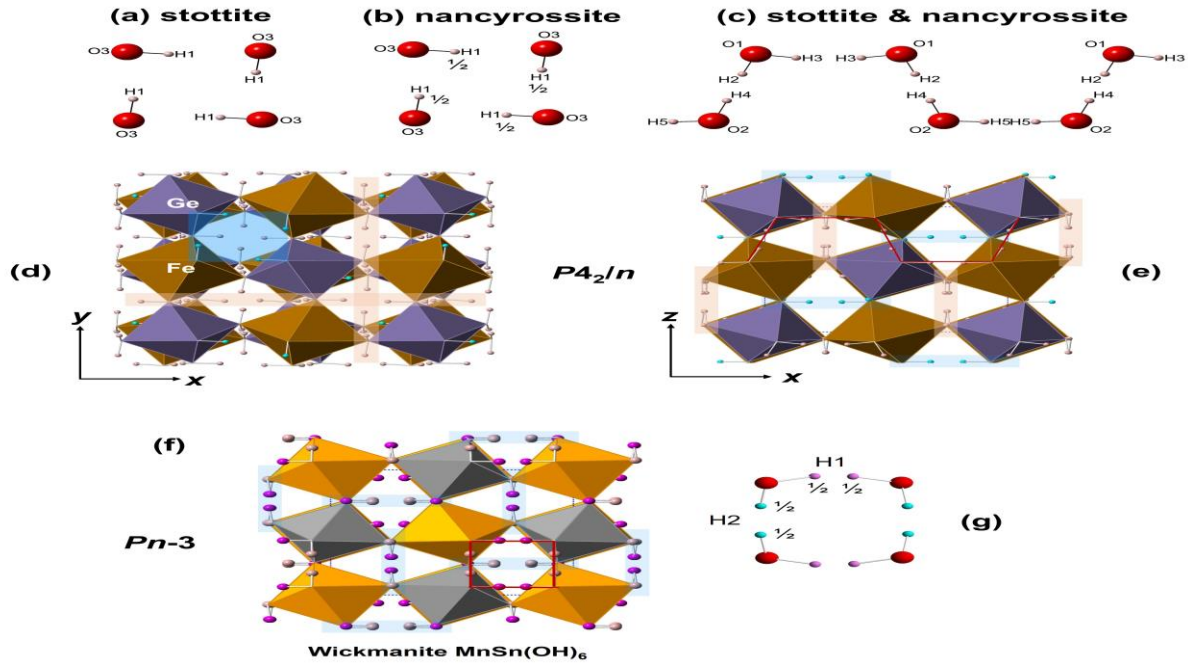

Figure 3. The Raman spectra of nancyrossite from Tsumeb (blue) compared with that of jeanbandyite from Hingston Quarry, Cornwall UK (purple). Both spectra have two broad bands in the (OH)-stretching region 2700-3600 cm^{-1}. At the top is the Raman spectrum of stottite from Tsumeb in which the five resolved OH bands lie within the same wavenumber range as the two broad bands of the nancyrossite and jeanbandyite spectra.

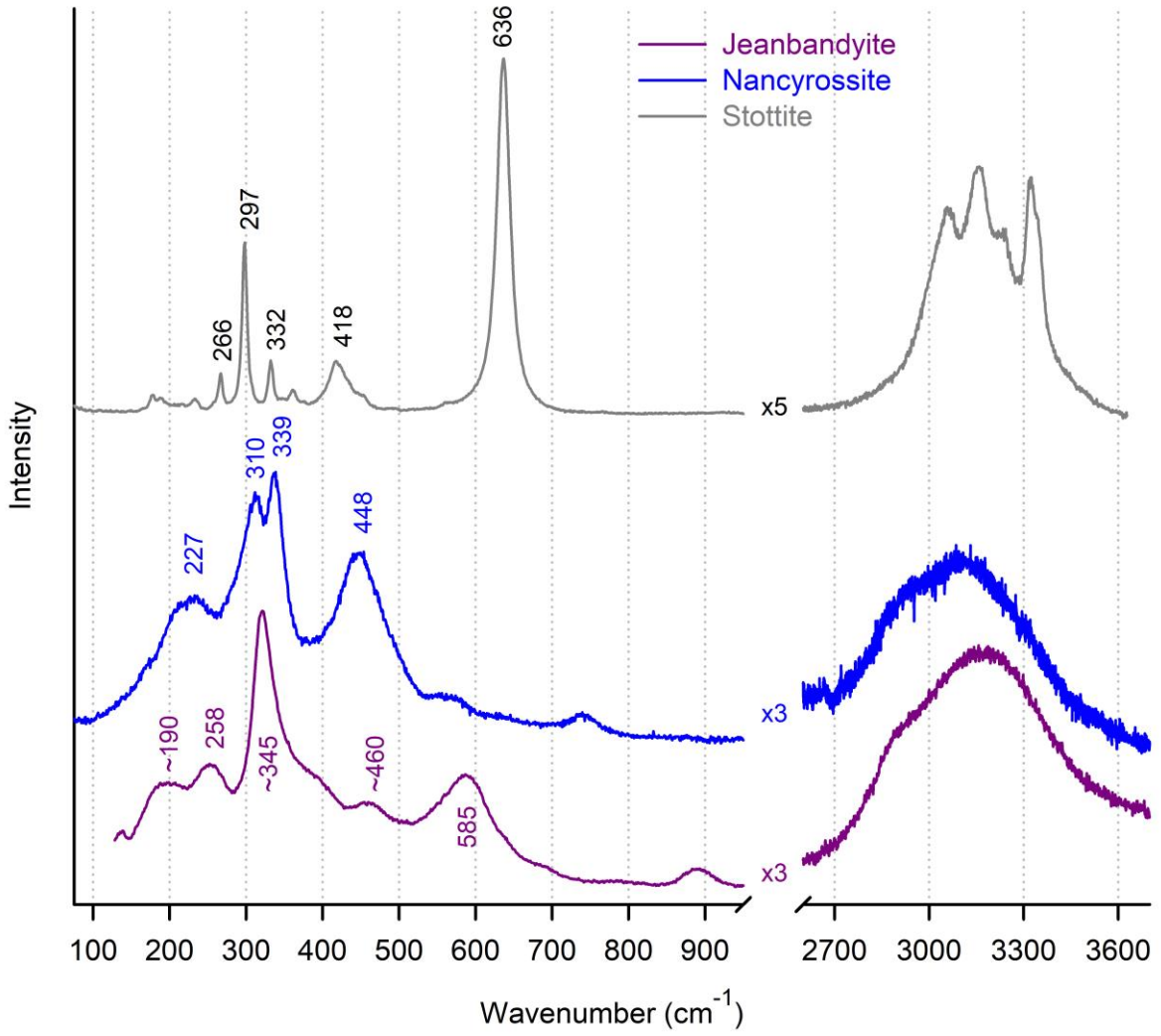

Table 1. Electron microprobe data for nancyrossite crystals #7 and #8.

Oxide	Mean wt %	Range	St..Dev (1σ)	Standard
		Crystal #7 (*n* = 23)		
Fe_2O_3	34.77	34.22 - 36.06	0.10	haematite
ZnO	1.08	1.16 - 1.31	0.02	sphalerite
GeO_2	44.90	43.70 - 45.62	0.71	Ge metal
Total	80.75			
		Crystal #8 (*n* = 11)		
Fe_2O_3	35.30	34.74 - 35.47	0.22	haematite
ZnO	1.24	1.03 - 1.23	0.04	sphalerite
GeO_2	44.70	43.84 - 45.94	0.54	Ge metal
Total	81.24			

Table 2. Calculated and measured powder XRD data for nancyrossite from a quasi-random pattern of the holotype crystal collected using a Gandolfi-type movement with Cu$K\alpha$ radiation. Only reflections with intensities above 5% are given.

d_{hkl} calc [Å]	d_{hkl} meas [Å]	I/I_{max} (calc)	I/I_{max} (meas)	h	k	l
4.2423	4.2437	6	6	1	1	1
3.6867	3.6885	100	100	2	0	0
3.6488	3.6489	46	31	0	0	2
2.6069	2.6082	17	27	2	2	0
2.5934	2.5941	39	53	2	0	2
2.3292	2.3303	5	9	3	0	1
2.3101	2.3102	5	9	1	0	3
2.2220	2.2221	7	12	3	1	1
2.1211	2.1219	17	27	2	2	2
1.8433	1.8443	16	29	4	0	0
1.8244	1.8244	7	15	0	0	4
1.6487	1.6496	17	31	4	2	0
1.6453	1.6460	19	37	4	0	2
1.6352	1.6353	18	38	2	0	4
1.5025	1.5031	24	36	4	2	2
1.4947	1.4950	13	21	2	2	4

Table 3. Information relating to data collection and structure refinement of nancyrossite (crystal #9) at 293K.

Crystal data	
Ideal formula	$FeGeO_6H_5$
Empirical formula (EMPA)	$Fe^{3+}_{1.01}Zn_{0.03}Ge_{0.98}O_6H_5$ (crystal 7) $Fe^{3+}_{1.01}Zn_{0.04}Ge_{0.98}O_6H_5$ (crystal 8)
Crystal 9 (holotype)	
Crystal system, space group	Tetragonal, $P4_2/n$ (No. 86)
a (Å)	7.37382(12)
c (Å)	7.29704(19)
V (Å^3)	396.764(16)
Z	4
D (calc) g/cm^3	3.842
μ mm^{-1}	11.158
Diffractometer	Xcalibur E (1K Eos detector)
Radiation	Mo$K\alpha$
Temperature (K)	293(2)
Scan type, frame-width (°), frame-time (s)	ω, 1.00, 100
Absorption correction	Multi-scan
T_{min}, T_{max}	0.8622, 1
Reflections used for cell, I >7σ(I)	2691
Reflections measured	11872
R_σ	0.011
Independent reflections	925
Independent reflections with I >2σ(I)	711
R_{int}	0.025
θ_{min}, θ_{max} (°)	2.762, 36.037
Index range	h ±12, k –12,+11, l ±11
Data completeness to 35°θ (%)	100
Refinement	
Reflections, parameters, restraints	925, 57, 5
$R_1[I > 2\sigma(I)]$, R_1(all)	0.022, 0.034
$wR_2[I > 2\sigma(I)]$, wR_2(all)	0.048, 0.051
$S(F^2)$	1.057
Reflection weighting coefficients a, b	0.0183, 0.3274
$(\Delta/\sigma)_{max}$	< 0.001
$\Delta\rho_{max}$, $\Delta\rho_{min}$ (e^- Å^{-3})	+0.67, -0.73

Table 4. Atom coordinates and equivalent-isotropic displacement parameters (Å^2) of nancyrossite (crystal 9). An overall U_{iso} was refined for the five H atoms; all H sites are half-occupied.

Site	*x/a*	*y/b*	*z/c*	U_{eq} /U_{iso}
Fe	0	0	0	0.01231(7)
Ge	½	0	0	0.00910(6)
O1	0.4510(2)	0.2409(2)	0.0804(2)	0.0132(2)
O2	0.2399(2)	0.5673(2)	0.0585(2)	0.0124(2)
O3	0.5649(2)	0.5699(2)	0.2595(1)	0.0115(2)
H1	0.679(2)	0.582(7)	0.258(7)	0.040(7)
H2	0.488(7)	0.243(7)	0.188 (4)	0.040(7)
H3	0.339(3)	0.246(8)	0.100(7)	0.040(7)
H4	0.238(7)	0.531(7)	0.168(4)	0.040(7)
H5	0.254(9)	0.679(3)	0.054(7)	0.040(7)

Table 5. Geometrical parameters for coordination polyhedra in nancyrossite.

Fe-O (Å)		Ge-O (Å)	
$O1^{x2}$	2.0310(12)	$O1^{x2}$	1.9050(12)
$O2^{x2}$	2.0265(12)	$O2^{x2}$	1.8861(12)
$O3^{x2}$	2.0202(10)	$O3^{x2}$	1.8904(10)
average	2.026	average	1.894
V(Å^3)	11.08	*V*(Å^3)	9.05
*DI**	0.0019	*DI*	0.0039
σ*	1.512	σ	0.623
λ*	1.0004	λ	1.0002

*Distortion Index (*DI*), bond-angle variance (σ) and quadratic elongation (λ) defined by Robinson et al. (1971).

Table 6. Unit cell parameters, structure refinement parameters, bond-lengths and octahedral volumes for crystals #7, #8 and #9.

crystal#	*a* (Å)	*c* (Å)	*V* (Å^3)	*R*1 (>2σ)	*GoF*	<Fe-O> (Å)	<Ge-O> (Å)	*V*(FeO$_6$) (Å^3)	*V*(GeO$_6$) (Å^3)
7	7.37620(10)	7.2965(2)	396.990(15)	0.0211	1.070	2.026	1.895	11.08	9.07
8	7.37429(11)	7.2942(2)	396.660(16)	0.0251	1.111	2.025	1.896	11.06	9.09
9	7.37382(12)	7.29704(19)	396.764(16)	0.0220	1.057	2.026	1.894	11.08	9.05

Table 7. Hydrogen bonding in nancyrossite (crystal #9) and stottite. The values for stottite were obtained from a refinement of a crystal used in the study by Kleppe et al. (2012). Distances in Å, angles in degrees.

nancyrossite

	O3(H1)···O3	O1(H2)···O2	O1(H3)···O1	O2(H4)···O1	O2(H5)···O2
d(O-H)	0.84(2)	0.83(2)	0.83(2)	0.84(2)	0.83(2)
d(H···O)	1.86(2)	1.95(2)	2.15(2)	1.94(2)	1.87(2)
d(O_D–O_A)	2.697(2)	2.775(2)	2.968(2)	2.775(2)	2.700(2)
∠O-H···O	174(5)	175(5)	166(5)	174(5)	174(6)

stottite

	O3(H1)···O3	O1(H2)···O2	O1(H3)···O1	O2(H4)···O1	O2(H5)···O2
d(O-H)	0.82(2)	0.84(2)	0.84(2)	0.84(2)	0.83(2)
d(H···O)	1.92(2)	2.00(2)	2.16(2)	2.00(2)	1.8(29)
d(O_D–O_A)	2.734(2)	2.824(2)	2.953(3)	2.824(2)	2.716(3)
∠O-H···O	173(3)	166(5)	157(5)	167(5)	173(5)

Table 8. Bond valence calculations for nancyrossite and stottite. Data for stottite are calculated from a refinement of the same crystal as that studied by Kleppe et al. (2012). Bond valence parameters for Fe^{2+}-O, Fe^{3+}-O and Ge-O bonds were taken from Brese and O'Keeffe (1991).

(a) nancyrossite

	Fe^{3+}	**Ge**	
O1	0.479 ×2↓	0.654 ×2↓	**1.133**
O2	0.484 ×2↓	0.689 ×2↓	**1.173**
O3	0.494 ×2↓	0.681 ×2↓	**1.175**
	2.914	**4.048**	

	Fe^{2+}	**Ge**	
O1	0.448 ×2↓	0.654 ×2↓	**1.102**
O2	0.453 ×2↓	0.689 ×2↓	**1.142**
O3	0.461 ×2↓	0.681 ×2↓	**1.142**
	2.724	**4.048**	

(b) stottite

	Fe^{2+}	**Ge**	
O1	0.326 ×2↓	0.658 ×2↓	**0.984**
O2	0.323 ×2↓	0.694 ×2↓	**1.017**
O3	0.344 ×2↓	0.683 ×2↓	**1.027**
	1.985	**4.070**	

Table 9. Nancyrossite and related minerals.

Mineral/Phase	Chemical formula	*B*, *B*'	SG	*a* (Å)	*b* (Å)	*c* (Å)	*V* (Å^3)	*V* BO_6 (Å^3)	*V* $B'O_6$ (Å^3)	Ref.
nancyrossite	$FeGeO_6H_5$	Fe^{3+}, Ge	$P4_2/n$	7.3738	-	7.2970	396.76	11.08	9.05	1
stottite	$FeGe(OH)_6$	Fe^{2+}, Ge	$P4_2/n$	7.5442	-	7.4560	424.36	13.13	9.07	2
zincostottite	$ZnGe(OH)_6$	Zn, Ge	$P4_2/n$	7.4522		7.4000	411.00	11.86	9.11	3
tetrawickmanite	$MnSn(OH)_6$	Mn^{2+}, Sn	$P4_2/n$	7.8655	-	7.7938	482.17	14.04	11.59	4
wickmanite	$MnSn(OH)_6$	Mn^{2+}, Sn	*Pn*-3	7.8754	-	-	488.45	14.09	11.57	4
synthetic	$FeSn(OH)_6$*	Fe^{2+}, Sn	*Pn*-3	7.83	-	-	480.05	-	-	5
jeanbandyite	$FeSnO(OH)_5$**	Fe^{3+}, Sn	*Pn*-3	7.6427	-	-	446.41	11.15	11.79	6
synthetic	$FeSnO(OH)_5$**	Fe^{3+}, Sn	*Pn*-3	7.64	-	-	445.94	-	-	5
bernalite	$Fe(OH)_3$	Fe^{3+}*	*Pmmn****	7.6191	7.6191	7.5534	438.48	10.80***	-	7

*A reliable structure for natanite is unavailable in the literature. Consequently, only the unit cell parameter and space group are shown here. **Formula given here as it is reported by Nakayama et al. (1977) and Welch and Kampf (2017). ***Bernalite has only a single non-equivalent Fe^{3+} site ($B = B'$) and is metrically tetragonal but structurally orthorhombic.

References: (1) This proposal; (2) Kleppe et al. (2012); (3) Kampf et al. (2025); (4) Lafuente et al. (2015); (5) Nakayama et al. (1977); (6) Welch and Kampf (2017); (7) Welch et al. (2005).